Nanoscale

ROYAL SOCIETY OF CHEMISTRY

COMMUNICATION

View Article Online
View Journal | View Issue

Cite this: *Nanoscale*, 2021, **13**, 14016

Received 27th April 2021,
Accepted 22nd July 2021

DOI: 10.1039/d1nr02674g

rsc.li/nanoscale

Spiral- and meridian-patterned spheres self-assembled from block copolymer/homopolymer binary systems†

Wenheng Xu,‡ Zhanwen Xu,‡ Chunhua Cai, * Jiaping Lin, * Liang Gao, Huimin Qi and Shaoliang Lin

Spiral nanostructures, mainly in the 2D form, have been observed in polymer self-assembly, while well-defined 3D spirals are rarely reported. Here we report that a binary system containing polypeptide-based block copolymers and homopolymers can self-assemble into well-defined spiral spheres (3D spirals), in which the homopolymers form the core and the copolymers form the spirals. Upon increasing the preparation temperature, meridian spheres were obtained. Mixing polypeptide block copolymers with opposite backbone chirality also leads to the formation of meridian spheres. In the meridian patterns, a tighter packing manner of the phenyl groups appended to the polypeptide blocks was observed, which is responsible for the spiral-to-meridian transitions. This work enriches the research of spiral assemblies and provides a facile route to switch chiral/achiral nanostructures by regulating the packing manner of the pendant groups.

The spiral form is a fundamental geometrical structure in nature, which attracts broad interest of communities from mathematics and physics to chemistry and materials.[1–5] Spiral structures possess both ordered and chiral characteristics endowing them with advanced and amazing functions such as magnetic properties, catalytic activity, signal enhancement of devices, and optical properties.[6–11] Self-assembly of block copolymers (BCPs) gives rise to varieties of ordered and chiral assemblies, such as helices and Moebius strips.[12–16] Recently, increasing attention has been paid to the spiral assemblies;[1,17–21] however, the formation mechanism of spirals has not been well clarified, and in-depth studies are desired to get well-defined spiral nanostructures. In addition, 2D spirals are observed in most cases, while the 3D forms, for example, spiral spheres, are rarely reported.

A spiral sphere, a typical 3D spiral nanostructure, is a kind of highly ordered form of stripe-pattern spheres. Usually, stripe spheres self-assembled from polymers possess a relatively low regularity.[22–24] In a droplet confinement, block copolymers could self-assemble into ordered stripes on particles, such as screw-like and ring-like stripes.[25–27] Additionally, as an achiral form of spiral spheres, meridian spheres, however, have not been observed in polymer self-assembly systems. It is a challenge to prepare highly ordered striped spheres in a simple solution system, *i.e.*, spiral spheres and meridian spheres through polymer self-assembly. Moreover, accessing various ordered nanostructures in a facile and gentle manner is also an attractive topic, which can not only enhance understanding of the self-assembly mechanism but also provide a facile route toward novel morphologies. Therefore, on a spiral sphere system, it should be very appealing to seek the possibility of accessing meridian patterns by regulating preparation conditions and also elucidate the mechanism behind the morphology transitions.

Herein, we report that a binary system containing poly(γ-benzyl-L-glutamate)-*block*-poly(ethylene glycol) (PBLG-*b*-PEG) rod-coil BCPs and polystyrene (PS) homopolymers is able to self-assemble into spiral and meridian spheres. They were prepared by a selective precipitation method. First, $PBLG_{75}$-*b*-PEG_{112} BCPs and PS_{62} homopolymers (the subscripts refer to the degree of polymerization, DP, of the corresponding block) were dissolved in a mixed solvent of tetrahydrofuran/*N*,*N*′-dimethylformamide (THF/DMF). For the characterization of the polymers, see Table S1 and Fig. S1 in the ESI.† The initial polymer concentration was 0.2 g L^{-1}, and the weight ratio of PBLG-*b*-PEG to PS is usually 3/7. Then, to 4 mL of the polymer solution, water (a selective solvent for the PEG blocks) was subsequently added at a rate of 0.04 mL min^{-1} under stirring (water content reaches 23.0 vol%), followed by dialyzing against water to remove the organic solvents. The effect of assembling temperature and the initial solvent composition

Shanghai Key Laboratory of Advanced Polymeric Materials, Key Laboratory for Ultrafine Materials of Ministry of Education, Frontiers Science Center for Materiobiology and Dynamic Chemistry, School of Materials Science and Engineering, East China University of Science and Technology, Shanghai 200237, China. E-mail: caichunhua@ecust.edu.cn, jlin@ecust.edu.cn

†Electronic supplementary information (ESI) available: Synthesis and characterisation of polymers; characterization of assemblies; influencing factors for surface nanostructures. See DOI: 10.1039/d1nr02674g

‡These authors contributed equally.

(volume fraction of DMF, f_{DMF}) on the surface pattern morphology is studied. In the study of the effect of temperature, all experimental procedures, including the processes of adding water and dialysis, were performed at a constant temperature.

Results and discussion

Fig. 1 shows SEM images of the samples prepared with f_{DMF} = 0.5 at various temperatures. Spherical aggregates with a diameter of about 650 nm were formed under these conditions; however, the surface pattern differs with each sample. As shown in Fig. 1a, when prepared at 20 °C, spiral spheres were obtained. The stripes, having a uniform width of about 38 nm, fully cover the spheres and wind in a left-handed direction indicating left-handed chirality of the spirals. Upon increasing the preparation temperature to 40 °C, spiral patterns were also observed (Fig. 1b); however, these spirals are straighter than those prepared at 20 °C. Upon further increasing the temperature to 60 °C, as shown in Fig. 1c, rather than chiral spirals, straight stripes on the spheres, *i.e.*, achiral meridian surface patterns, were observed. Though 3D spirals have been reported in some studies,[20] the meridian pattern, a special form of the 3D spiral, has not been observed in BCP self-assembly systems.

Since these spirals are uniform in diameter and tightly packed with each other, we infer that these spirals are Archimedean spirals on spheres.[28,29] The spirals were fitted with the polar equation of Archimedean spirals on spheres. The equation of Archimedean spirals on spheres in the spherical coordinates is given by:

$$\varphi - \varphi_0 = a(\theta - \theta_0) \quad (1)$$

where θ is the polar angle from the positive z-axis and φ is the azimuthal angle in the xy-plane from the x-axis, as shown in Fig. 1d. φ_0 and θ_0 are the constants determining the start point of the spiral. The increment ratio of φ to θ gives a spinning speed (a). A smaller a value corresponds to a straighter spiral, and for the meridian patterns, a = 0.

Fig. 1e–g show the fitting traces of various spirals. As can be seen, these spirals are a good fit with the Archimedean spiral model, which indicates a highly ordered arrangement of these spirals on the surfaces of spheres. The slope of the fitting trace corresponds to the spinning speed of the spirals (the a value), which decreases from 4.5 to 2.6 and then to 0.011 with the preparation temperature increasing from 20 to 40 °C and then to 60 °C. Such a variation of the spinning speed corresponds to the spiral-to-meridian morphology transition. Furthermore, by combining the a value, the diameter of the sphere (D_s), and the width of spirals (w), we can obtain structural parameters including screw pitch (p, $p = \pi D_s/a$) and strand number (n, $n = p/w$) of the spirals. The D_s and w values were obtained by measuring the striped spheres in the SEM images (the size of the spheres was also examined by dynamic light scattering, for detailed information, see Fig. S2†). It was found that all these spirals are multi-stranded, and both the p

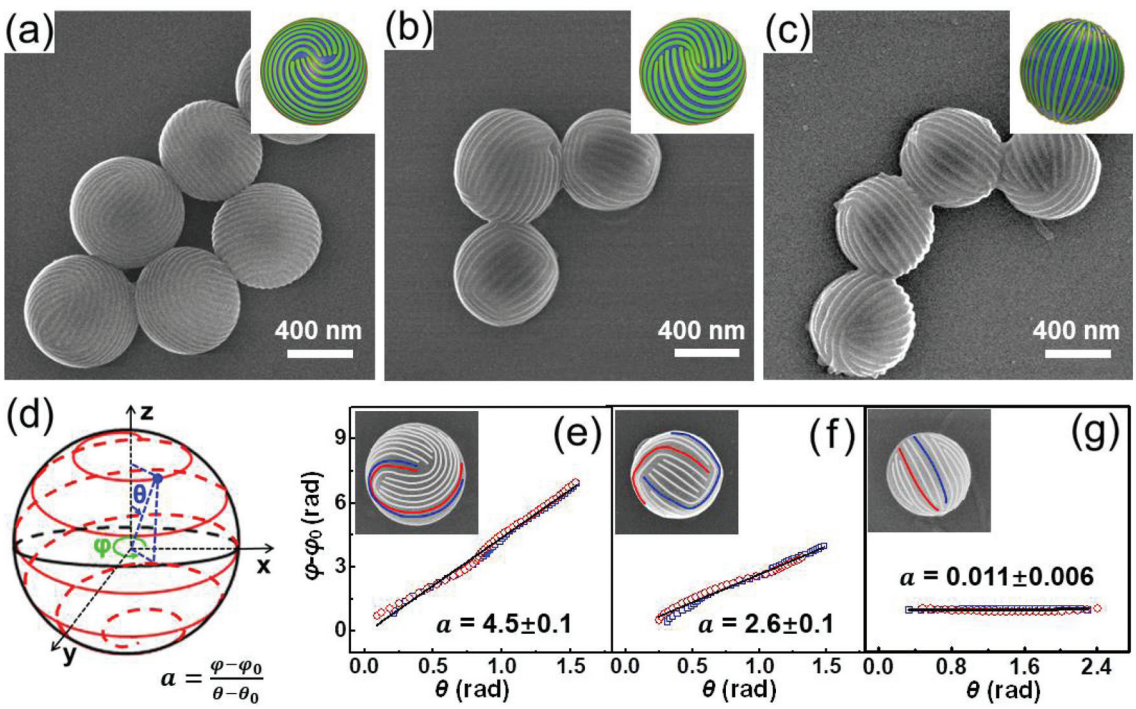

Fig. 1 (a–c) SEM images of left-handed spiral and achiral meridian spheres self-assembled from $PBLG_{75}$-*b*-PEG_{112} BCPs and PS_{62} homopolymers with f_{DMF} = 0.5 at various temperatures: (a) 20 °C; (b) 40 °C; and (c) 60 °C. (d) Scheme for the Archimedean spiral sphere. (e–g) Plot of the azimuthal angle $\varphi-\varphi_0$ *versus* the polar angle $\theta-\theta_0$ for the surface patterns. The inset images in (e–g) correspond to samples shown in (a–c), respectively.

Table 1 Parameter information of the surface stripes

Parameters	T = 20 °C f_{DMF} = 0.5	T = 40 °C f_{DMF} = 0.5	T = 60 °C f_{DMF} = 0.5	T = 20 °C f_{DMF} = 0.3	T = 20 °C f_{DMF} = 0.7
Morphology	Spiral	Spiral	Meridian	Spiral	Spiral
a value	4.5 ± 0.1	2.6 ± 0.1	0.011 ± 0.006	11.5 ± 0.1	2.4 ± 0.1
D_s [a]	681 ± 25	660 ± 23	630 ± 10	644 ± 17	660 ± 22
Screw pitch/nm	475 ± 3	797 ± 5	—[b]	176 ± 1	864 ± 5
Strand number	13 ± 1	21 ± 2	—[b]	5 ± 1	23 ± 2

[a] The size of the spheres was also characterized by dynamic light scattering (DLS), which gives a similar size to the SEM observations. [b] From the definition, meridians have infinite p and n values.

and n values increase with the decrease of the a value. For example, for the spirals with a = 4.5, the p and n values are 475 nm and 13, respectively, and with the decrease of the a value to 2.6, the p and n values increase to about 797 nm and 21, respectively. For the meridians, according to the definition of the spirals, they have infinite p and n values. The detailed characteristics of these multi-strand spirals are summarized in Table 1.

The initial solvent nature exerts a considerable effect on the surface patterns. The results are presented in Fig. 2 and Table 1. When prepared with f_{DMF} = 0.3, spiral patterns can also be observed which have an a value of 11.5 (Fig. 2a). When prepared with f_{DMF} = 0.7, straighter spirals with a smaller a value (a = 2.4) were obtained (Fig. 2c). The fitting traces are presented in the ESI (Fig. S3†). These results revealed that the a value of the spirals decreases with increasing f_{DMF} in the initial solvent. In addition, among the spiral spheres prepared with f_{DMF} = 0.3, achiral latitudinal stripe spheres are occasionally observed (Fig. 2b). By examining over 100 particles, latitudinal spheres were found to account for about 4.7% of the number. Note that the latitudinal spheres are usually prepared through a confined self-assembly approach,[30] which is the first report regarding bulk solution self-assembly of latitudinal spheres from block copolymers.

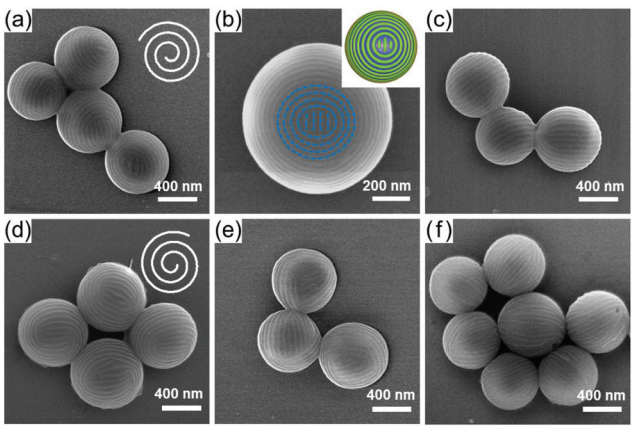

Fig. 2 (a–c) SEM images of striped spheres self-assembled from $PBLG_{75}$-*b*-PEG_{112} BCPs and PS_{62} homopolymers with various f_{DMF} values: (a and b) f_{DMF} = 0.3 and (c) f_{DMF} = 0.7. T = 20 °C. (d–f) Striped spheres self-assembled from $PBLG_{75}$-*b*-PEG_{112}/$PBDG_{83}$-*b*-PEG_{112}/PS_{62} mixtures with various PBLG-*b*-PEG/PBDG-*b*-PEG weight ratios: (d) 0/3, (e) 1/2, and (f) 1.5/1.5. f_{DMF} = 0.3, T = 20 °C.

The effect of the DP of the polymers on the surface pattern is also studied. The DP of both PBLG-*b*-PEG BCPs and PS homopolymers exerts no significant effect on the overall morphology of the assemblies. The width of the stripes increases approximately linearly with the DP of the PBLG blocks. For example, for the samples prepared with f_{DMF} = 0.3 and T = 20 °C, the width of the stripes formed by $PBLG_{75}$-*b*-PEG_{112} is about 38 nm, narrower stripes of about 21 nm were formed by $PBLG_{41}$-*b*-PEG_{112} BCPs, and wider stripes of about 49 nm were formed by $PBLG_{111}$-*b*-PEG_{112} BCPs. From the length of the BCPs and the width of the stripes, a head-to-head packing mode of the BCPs in the stripes is deduced. Detailed results are presented in the ESI (Fig. S4 and S5†).

As revealed above, the PBLG-*b*-PEG Archimedean spirals possess left-handed chirality, which could be related to the chiral feature of the PBLG blocks (the PBLG backbone takes a right-handed α-helix conformation). Such assumption was verified by the formation of right-handed Archimedean spirals by $PBDG_{83}$-*b*-PEG_{112}/PS_{62} mixtures [PBDG: poly(γ-benzyl-D-glutamate) takes a left-handed α-helix conformation]. Fig. 2d shows the right-handed spirals (a = −12.8, the "−" corresponds to right-handed spirals) formed by $PBDG_{83}$-*b*-PEG_{112}/PS_{62} with f_{DMF} = 0.3 at 20 °C. The surface pattern can be regulated by mixing $PBLG_{75}$-*b*-PEG_{112} and $PBDG_{83}$-*b*-PEG_{112} BCPs under similar preparation conditions. For example, spiral spheres formed by $PBLG_{75}$-*b*-PEG_{112}/$PBDG_{83}$-*b*-PEG_{112}/PS_{62} mixtures (weight ratio: 1/2/7) have a smaller a value of −8.0 (Fig. 2e), and achiral meridian spheres were formed by $PBLG_{75}$-*b*-PEG_{112}/$PBDG_{83}$-*b*-PEG_{112}/PS_{62} mixtures (weight ratio: 1.5/1.5/7) (Fig. 2f). When the weight ratio of $PBLG_{75}$-*b*-PEG_{112} BCPs surpasses that of $PBDG_{83}$-*b*-PEG_{112} BCPs in the mixtures, left-handed spiral spheres were prepared. For more results, see Fig. S6 and S7 in the ESI.†

Apart from the surface patterns, the inner structure also should be explored. For the PBLG-*b*-PEG/PS spiral spheres, it is deduced that the PS homopolymers form the inner core and the PBLG-*b*-PEG BCPs self-assemble into the surface spirals. To address such an issue, we first studied the self-assembly morphology of $PBLG_{75}$-*b*-PEG_{112} BCPs and PS_{62} homopolymers, respectively (the assembly conditions: polymer concen-

tration = 0.2 g L^{-1}, T = 20 °C, f_{DMF} = 0.3). It was found that $PBLG_{75}$-*b*-PEG_{112} BCPs form small spherical aggregates, and PS_{62} homopolymers form large spheres. These results prove that the formation of the spiral spheres is the result of the co-assembly of PBLG-*b*-PEG BCPs and PS homopolymers, and the surface spirals could be self-assembled by the BCPs.

We then conducted a two-step self-assembly experiment to further confirm the structure of the spiral spheres (Fig. 3a). In the first step, to solutions of $PBLG_{75}$-*b*-PEG_{112} BCPs (1.2 mL, 0.2 g L^{-1}, f_{DMF} = 0.3) and PS_{62} homopolymers (2.8 mL, 0.2 g L^{-1}, f_{DMF} = 0.3) respectively, 13.0 vol% of water was dropped at a rate of 0.04 mL min^{-1}. Note: the critical water contents of PS_{62} homopolymers and $PBLG_{75}$-*b*-PEG_{112} BCPs were 9.3 and 16.1 vol%, respectively (Fig. S8 in the ESI†). In this situation, the PS homopolymers formed spheres (Fig. 3b), while the PBLG-*b*-PEG BCPs were still dispersed in the solution. In the second step, these two polymer solutions were mixed together, and more water was added to reach the final water content of 23.0 vol%. After dialysing against water, as shown in Fig. 3c, spiral spheres similar to those prepared with the direct self-assembly process were obtained. By comparing the diameter of the blank PS spheres and that of the PBLG-*b*-PEG/PS spiral spheres, the thickness of the PBLG-*b*-PEG shell was determined to be about 24 nm (the inset of Fig. 3c). With the decrease of the BCPs/homopolymer feeding weight ratio to 2/8 and 1/9, the thickness of the PBLG-*b*-PEG shell decreases to *ca.* 18 (Fig. 3d) and 9 nm (Fig. 3e), respectively. In addition, by controlling the adding rate of water in the first step, the size of the PS spheres as well as the spiral spheres can be readily adjusted (Fig. S9 in the ESI†).

From these above-mentioned results, the overall structure of the spiral spheres can be well explicated. As illustrated by the cartoon on the right of Fig. 3a, the PS homopolymers and BCPs respectively formed cores and surface spirals; in the spirals, the BCPs pack in a head-to-head mode and the direction of the BCP axis is parallel with the sphere surface.

In the following content, the mechanisms for the transition between chiral spirals and achiral meridians will be analysed. Under the current assembly conditions (*i.e.*, with THF and DMF as solvents, and in the temperature range of 20–60 °C), PBLG chain backbones retain their rigid α-helix conformation.[31,32] Therefore, the possibility that the PBLG conformation transition induced the surface morphology transition can be ruled out. Consequently, the possible reason for such surface pattern transitions could be the different packing modes of the block copolymers under different conditions.

Synchrotron radiation wide-angle X-ray diffraction (WAXS) is a powerful tool to check the chain packing information of assemblies.[33–36] In this work, various samples prepared under different conditions were employed for the WAXS testing. Fig. 4a shows the WAXS pattern of spiral spheres formed by $PBLG_{75}$-*b*-PEG_{112}/PS_{62} with f_{DMF} = 0.5 at 20 °C. The multiple diffraction rings in the WAXS pattern indicate ordered periodic nanostructures. As shown in Fig. 4b, the characteristic diffraction peak at q_1 = 4.41 nm^{-1} corresponds to the distance d = 1.42 nm, which is ascribed to the distance between adjacent

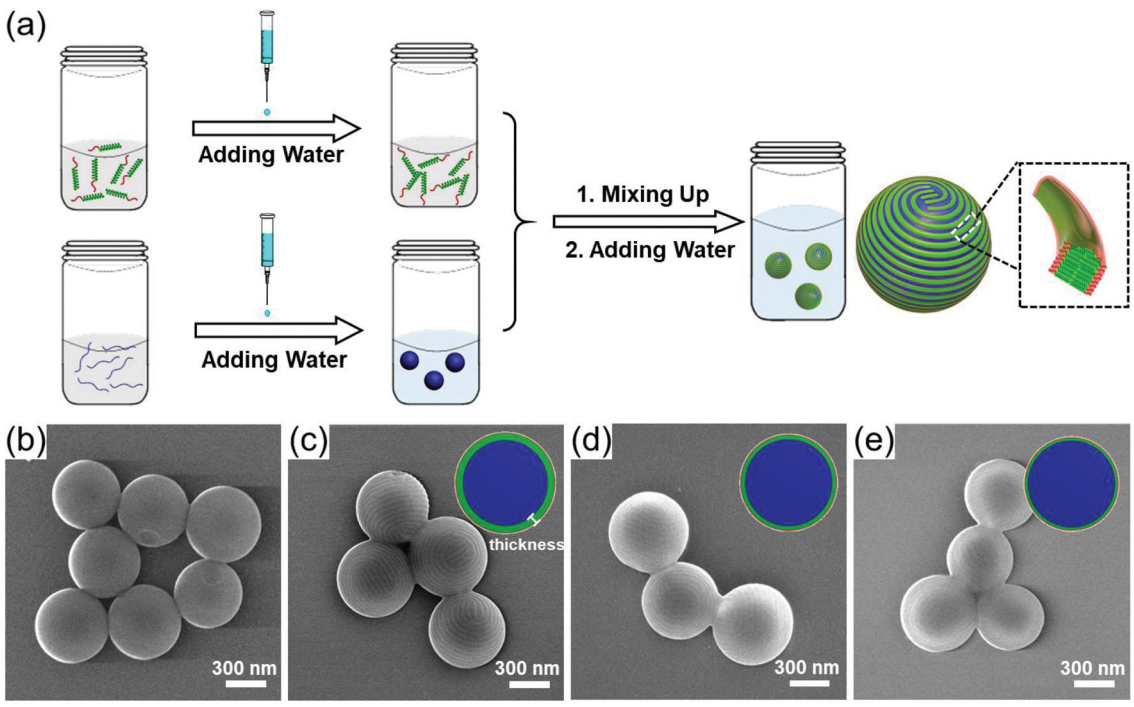

Fig. 3 (a) Representation of the fabrication of $PBLG_{75}$-*b*-PEG_{112}/PS_{62} spiral spheres through a two-step self-assembly approach. The scheme on the right presents a structure of the spiral sphere as well as the spiral. (b) SEM image of plain spheres assembled from PS homopolymers in the first step. (c–e) SEM images of spiral spheres prepared in the second step with various BCP/homopolymer feeding weight ratios: (c) 3/7, (d) 2/8, and (e) 1/9. The insets represent schemes of the assemblies, and the blue, green, and red layers represent PS, PBLG, and PEG chains, respectively.

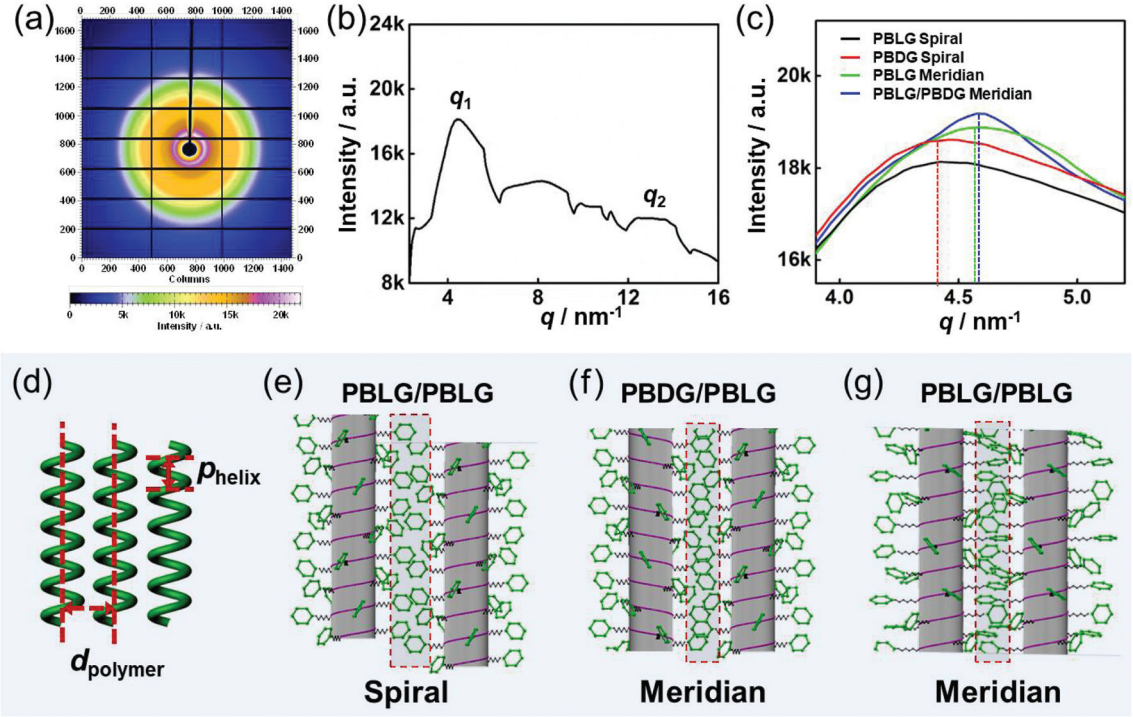

Fig. 4 (a) WAXS pattern and (b) WAXS spectrum of the spiral spheres formed by $PBLG_{75}$-*b*-PEG_{112}/PS_{62} mixtures with f_{DMF} = 0.5 at 20 °C (PBLG spiral). (c) WAXS spectra of various samples. Note: the PBDG spiral is formed by $PBDG_{82}$-*b*-PEG_{112}/PS_{62} mixtures with f_{DMF} = 0.5 at 20 °C; the PBLG meridian is formed by $PBLG_{75}$-*b*-PEG_{112}/PS_{62} mixtures with f_{DMF} = 0.5 at 60 °C; and the PBLG/PBDG meridian is formed by $PBLG_{75}$-*b*-PEG_{112}/$PBDG_{82}$-*b*-PEG_{112}/PS_{62} mixtures with f_{DMF} = 0.5 at 20 °C. (d) Scheme of the parallel packing mode of PBLG chains (the phenyl groups are omitted in the scheme for clarity). $d_{polymer}$ and p_{helix} represent the distance of adjacent PBLG chains and the pitch of the PBLG helix, respectively. (e–f) Schemes for the packing manner of the PBLG backbone and pendant phenyl groups in different structures: (e) PBLG spiral, (f) PBLG/PBDG meridian, and (g) PBLG meridian. The dashed red lines in (e–g) indicate the packing areas of the phenyl groups.

PBLG chains ($d_{polymer}$) in the spirals. As reported in the literature, the characteristic q value of the α-helix conformation of PBLG segments (p_{helix}) is usually around 11–13 nm^{-1}.[37–39] However, a flat-top peak (q_2) at 12–14 nm^{-1} was observed, which could be an overlap of both the higher order peak of 4.41 nm^{-1} (for example, q = 13.23 nm^{-1}) and the characteristic q value of the PBLG helix. Nevertheless, due to the broad hump of the peak, the characteristic q value of the PBLG helix could be confirmed. The definitions for $d_{polymer}$ and p_{helix} are shown in Fig. 4d.

Similar WAXS patterns were observed for the samples prepared under different conditions (f_{DMF} = 0.5 is fixed); however, the q_1 value varies for different samples. As shown in Fig. 4c, the q_1 value for spiral spheres formed by $PBDG_{83}$-*b*-PEG_{112}/PS_{62} at 20 °C (PBDG spiral) is 4.41 nm^{-1}, which is the same as that of the $PBLG_{75}$-*b*-PEG_{112}/PS_{62} spirals prepared at 20 °C (PBLG spiral), indicating a similar packing mode of the polymers in the spirals prepared under similar conditions, while for the meridian spheres formed by $PBLG_{75}$-*b*-PEG_{112}/PS_{62} at 60 °C (PBLG meridian), the q_1 value is found at 4.61 nm^{-1} ($d_{polymer}$ = 1.36 nm). A similar q_1 value of 4.65 nm^{-1} ($d_{polymer}$ = 1.35 nm) was observed for the meridian spheres formed by $PBLG_{75}$-*b*-PEG_{112}/$PBDG_{83}$-*b*-PEG_{112}/PS_{62} mixtures at 20 °C (PBLG/PBDG meridian). These results revealed that the polypeptide chains are packed more compactly in the meridians than in the spirals.

Based on these above-mentioned experimental results, the packing modes of the BCPs in the spirals and meridians are proposed (Fig. 4e–g). For the PBLG spirals (or PBDG spirals), as shown in Fig. 4e, the polypeptide blocks arrange in a chiral manner forming spirals. Due to the opposite chirality of PBLG and PBDG block backbones, the PBLG-*b*-PEG and PBDG-*b*-PEG BCPs packed in opposite fashions resulting in spirals with opposite chirality. For the achiral meridians formed by PBLG-*b*-PEG/PBDG-*b*-PEG mixtures (PBLG/PBDG meridians), since the distance between polypeptide chains ($d_{polymer}$) is slightly smaller, the PBLG and PBDG chains are deduced to be packed alternately, and the pendant phenyl groups from adjacent polypeptide chains should overlap with each other. Such a packing mode is illustrated in Fig. 4f. Note that a compact packing of chirality stereoisomers has also been reported in the literature.[40,41]

Similar to that observed in the PBLG-*b*-PEG/PBDG-*b*-PEG meridians, for the meridians formed by PBLG-*b*-PEG or PBDG-*b*-PEG BCPs under a higher preparation temperature, the $d_{polymer}$ is also smaller than that in the PBLG-*b*-PEG or PBDG-*b*-PEG spirals. Therefore, in the PBLG-*b*-PEG (or PBDG-*b*-PEG) meridians, it is deduced that the pendant phenyl groups from

adjacent chains should also be overlapped. The reasons are analysed as follows. At higher temperatures, the solvent solubility to polymers increases; therefore, the pendant phenyl groups are more solvated. The higher solvated state of the phenyl groups could facilitate their interchain overlapping. As a result, as illustrated in Fig. 4g, the $d_{polymer}$ value is decreased. Such a tight packing of phenyl groups could restrain the chirality transfer from the polypeptide backbone to the stripes; as a consequence, achiral meridians rather than chiral spirals were formed. In addition, both THF and DMF are good solvents for the BCPs, but the phenyl groups were more highly solvated in DMF,[31,42–44] which explains the formation of PBLG-*b*-PEG spirals with a lower chirality using a DMF-rich initial solvent (see Fig. 2a–c and Table 1).

Conclusions

In summary, uniform spiral spheres (3D spirals) were self-assembled from a binary system containing PBLG-*b*-PEG BCPs and PS homopolymers in a selective solvent. The PS homopolymers formed an inner sphere, on which the PBLG-*b*-PEG BCPs self-assembled into surface spirals. The chirality of the spirals is readily adjusted for the preparation temperature and initial solvent nature. Under higher preparation temperatures, the surface morphology can transform from the chiral spirals to achiral meridians. Mixing polypeptide block copolymers with opposite chirality also induces the spiral-to-meridian transition. Synchrotron radiation WAXS testing revealed that the distance between adjacent polypeptide chains in the meridians is smaller than that in the spirals, which is induced by the tighter packing manner of the phenyl groups appended to polypeptide backbones. This work not only presents novel surface-patterned assemblies including chiral spirals and achiral meridians, but also enriches our toolbox in controlling assembly morphologies by subtly adjusting the packing manner of the pendant groups.

Methods

Preparation of assemblies

Spiral and meridian patterned assemblies were prepared by the self-assembly of PBLG-*b*-PEG rod-coil BCPs and coil PS homopolymers. First, PBLG-*b*-PEG BCPs and PS homopolymers were dissolved in THF/DMF mixtures. The concentrations of the PBLG-*b*-PEG BCPs and PS homopolymers were the same, 0.2 g L^{-1}. Then, 1.2 mL of the PBLG-*b*-PEG BCP solution and 2.8 mL of the PS homopolymer solution were mixed together. To the solution, 1.2 mL of deionized water, a selective solvent for PEG blocks, was dropped at a rate of *ca.* 0.04 mL min^{-1} with stirring. After being stabilized for about 30 min, the solution was dialyzed against deionized water for 3 days to remove organic solvents. After dialysis, an aqueous solution of assemblies with a striped surface pattern was obtained. In the study of the effect of temperature, all experimental procedures, including the processes of adding water and dialysis, were performed at a constant temperature. The polymer solutions, water for micellization, and water for dialysis were stored at a corresponding temperature for more than 4 h before use.

Characterization of assemblies

The morphologies of the assemblies were characterized by Field Emission SEM (S4800, Hitachi). The sample was prepared by placing drops of solution on a Si wafer and then dried at room temperature. Before observation, the samples were sputtered with platinum. Synchrotron radiation WAXS measurement was performed at beamline BL16B1 of the Shanghai Synchrotron Radiation Facility. The wavelength of the X-ray was 0.124 nm (E = 10 keV), and the distance of the sample to a detector for WAXS was calibrated to be 207.51 mm. The exposure time was 60 s. A two-dimensional WAXS pattern was collected with a Mar165 CCD detector (2048 × 2048 pixels with a pixel size of 80 μm). The WAXS data were analyzed with Fit2D software from the European Synchrotron Radiation Facility. The *d*-spacing values were calculated from Bragg's law $d = 2\pi/q$.[33]

Conflicts of interest

There are no conflicts to declare.

Acknowledgements

This work was supported by the National Natural Science Foundation of China (52073095, 51621002, 51833003, and 51573049) and the project of Shanghai Municipality (20ZR1471300). Support of the Shanghai Synchrotron Radiation Facility, Beamline BL16B1 (2019-SSRF-PT-011602) for WAXS testing is also appreciated.

Notes and references

1 J. Malthête, J. Jacques, N. H. Tinh and C. Destrade, *Nature*, 1982, **298**, 46–48.
2 N. Sasaki, M. F. Mabesoone, J. Kikkawa, T. Fukui, N. Shioya, T. Shimoaka, T. Hasegawa, H. Takagi, R. Haruki and N. Shimizu, *Nat. Commun.*, 2020, **11**, 3578.
3 Y. Zhao, C. Zhang, D. D. Kohler, J. M. Scheeler, J. C. Wright, P. M. Voyles and S. Jin, *Science*, 2020, **370**, 442–445.
4 J. Yuan, X. Lu, Q. Li, Z. Lü and Q. Lu, *Angew. Chem., Int. Ed.*, 2021, **60**, 12308–12312.
5 H. Y. Hsueh, C. T. Yao and R. M. Ho, *Chem. Soc. Rev.*, 2015, **44**, 1974–2018.
6 J. Trevino, H. Cao and L. Dal Negro, *Nano Lett.*, 2011, **11**, 2008–2016.
7 S. H. Wibowo, A. Sulistio, E. H. Wong, A. Blencowe and G. G. Qiao, *Chem. Commun.*, 2014, **50**, 4971–4988.
8 Y. Zheng, L. Lin, X. Ye, F. Guo and X. Wang, *Angew. Chem., Int. Ed.*, 2014, **53**, 11926–11930.

9 T. Kan, A. Isozaki, N. Kanda, N. Nemoto, K. Konishi, H. Takahashi, M. Kuwata-Gonokami, K. Matsumoto and I. Shimoyama, *Nat. Commun.*, 2015, **6**, 8422.
10 Y. He, S. Chen, L. Nie, Z. Sun, X. Wu and W. Liu, *Nano Lett.*, 2020, **20**, 7136–7143.
11 A. R. Mazo, S. Allison-Logan, F. Karimi, N. J.-A. Chan, W. Qiu, W. Duan, N. M. O'Brien-Simpson and G. G. Qiao, *Chem. Soc. Rev.*, 2020, **49**, 4737–4834.
12 C. Cai, J. Lin, Y. Lu, Q. Zhang and L. Wang, *Chem. Soc. Rev.*, 2016, **45**, 5985–6012.
13 E. Yashima, N. Ousaka, D. Taura, K. Shimomura, T. Ikai and K. Maeda, *Chem. Rev.*, 2016, **116**, 13752–13990.
14 Z. Geng, B. Xiong, L. Wang, K. Wang, M. Ren, L. Zhang, J. Zhu and Z. Yang, *Nat. Commun.*, 2019, **10**, 4090.
15 G. Ouyang, L. Ji, Y. Jiang, F. Würthner and M. Liu, *Nat. Commun.*, 2020, **11**, 5910.
16 W. Xu, Z. Xu, C. Cai, J. Lin, S. Zhang, L. Zhang, S. Lin, Y. Yao and H. Qi, *J. Phys. Chem. Lett.*, 2019, **10**, 6375–6381.
17 K. Akagi, G. Piao, S. Kaneko, K. Sakamaki, H. Shirakawa and M. Kyotani, *Science*, 1998, **282**, 1683–1686.
18 T. Mori and K. Akagi, *Macromolecules*, 2013, **46**, 6699–6711.
19 H. K. Choi, J.-B. Chang, A. F. Hannon, J. K. Yang, K. K. Berggren, A. Alexander-Katz and C. A. Ross, *Nano Futures*, 2017, **1**, 015001.
20 C. D. Vacogne, C. Wei, K. Tauer and H. Schlaad, *J. Am. Chem. Soc.*, 2018, **140**, 11387–11394.
21 K.-C. Yang and R.-M. Ho, *ACS Macro Lett.*, 2020, **9**, 1130–1134.
22 N. J. Penfold, Y. Ning, P. Verstraete, J. Smets and S. P. Armes, *Chem. Sci.*, 2016, **7**, 6894–6904.
23 Y. Hirai, T. Wakiya and H. Yabu, *Polym. Chem.*, 2017, **8**, 1754–1759.
24 Y. Liu, W. Hou and H. Zhao, *Macromolecules*, 2020, **53**, 5001–5014.
25 S. J. Jeon, G. R. Yi and S. M. Yang, *Adv. Mater.*, 2008, **20**, 4103–4108.
26 T. Higuchi, A. Tajima, K. Motoyoshi, H. Yabu and M. Shimomura, *Angew. Chem., Int. Ed.*, 2008, **47**, 8044–8046.
27 T. Higuchi, K. Motoyoshi, H. Sugimori, H. Jinnai, H. Yabu and M. Shimomura, *Macromol. Rapid Commun.*, 2010, **31**, 1773–1778.
28 S. K. Khamas, *IEEE Trans. Antennas Propag.*, 2008, **56**, 345–352.
29 R. Sigrist and P. Matthews, *SIAM J. Appl. Dyn. Syst.*, 2011, **10**, 1177–1211.
30 R. Deng, F. Liang, W. Li, Z. Yang and J. Zhu, *Macromolecules*, 2013, **46**, 7012–7017.
31 E. Ibarboure, J. Rodríguez-Hernández and E. Papon, *Polym. Chem.*, 2006, **44**, 4668–4679.
32 C. Cai, J. Lin, T. Chen and X. Tian, *Langmuir*, 2010, **26**, 2791–2797.
33 J. S. Haataja, N. Houbenov, H. Iatrou, N. Hadjichristidis, A. Karatzas, C. F. Faul, P. Rannou and O. Ikkala, *Biomacromolecules*, 2012, **13**, 3572–3580.
34 D. Presa-Soto, G. A. Carriedo, R. de la Campa and A. Presa Soto, *Angew. Chem., Int. Ed.*, 2016, **55**, 10102–10107.
35 C.-C. Tsai, Z. Gan, T. Chen and S.-W. Kuo, *Macromolecules*, 2018, **51**, 3017–3029.
36 Y. H. Lee, Y. L. Yang, W. C. Yen, W. F. Su and C. A. Dai, *Nanoscale*, 2014, **6**, 2194–2200.
37 P. Papadopoulos, G. Floudas, H. A. Klok, I. Schnell and T. Pakula, *Biomacromolecules*, 2004, **5**, 81–91.
38 J. H. Wang, C. C. Cheng, Y. C. Yen, C. C. Miao and F. C. Chang, *Soft Matter*, 2012, **8**, 3747–3750.
39 L. Gao, H. Gao, J. Lin, L. Wang, X.-S. Wang, C. Yang and S. Lin, *Macromolecules*, 2020, **53**, 8992–8999.
40 C. Robinson, J. Ward and R. Beevers, *Discuss. Faraday Soc.*, 1958, **25**, 29–42.
41 F. Xu, I. J. Khan, K. McGuinness, A. S. Parmar, T. Silva, N. S. Murthy and V. Nanda, *J. Am. Chem. Soc.*, 2013, **135**, 18762–18765.
42 H. Schlaad, B. Smarsly and I. Below, *Macromolecules*, 2006, **39**, 4631–4632.
43 C.-J. Huang and F.-C. Chang, *Macromolecules*, 2008, **41**, 7041–7052.
44 C. Cai, J. Lin, X. Zhu, S. Gong, X.-S. Wang and L. Wang, *Macromolecules*, 2016, **49**, 15–22.

